Korean J. Chem. Eng., 39(9), 2345-2352 (2022)
DOI: 10.1007/s11814-022-1166-4

pISSN: 0256-1115
eISSN: 1975-7220

Chlorination behavior of $Li(Ni_{1/3}Co_{1/3}Mn_{1/3})O_2$

Min Ku Jeon*,,†, Sung-Wook Kim*, Maengkyo Oh*,***, Hee-Chul Eun*,**, and Keunkyoung Lee***

*Decommissioning Technology Research Division, Korea Atomic Energy Research Institute,
111, Daedeok-daero 989, Yuseong-gu, Daejeon 34057, Korea
**Department of Quantum Energy Chemical Engineering, University of Science and Technology,
217, Gajeong-ro, Yuseong-gu, Daejeon 34113, Korea
***Department of Chemical and Biomolecular Engineering, Yonsei University,
50 Yonsei-ro, Seodaemun-gu, Seoul 03722, Korea
(*Received 16 February 2022 • Revised 31 March 2022 • Accepted 6 May 2022*)

Abstract−The chlorination behavior of $Li(Ni_{1/3}Co_{1/3}Mn_{1/3})O_2$ (NCM) was investigated as a function of the reaction temperature (400-600 °C) and time (1-8 h) for application in a chlorination-based recycling process. Structural analysis results revealed that chlorination leads to a sequential transition from a hexagonal $LiMO_2$ structure to a hexagonal $Li_{1-x'}MO_{2-y'}$ (observed only at 400 °C), a hexagonal $Li_{1-x}MO_{2-y}$ ($x \geq x'$, $y \geq y'$, at 400-600 °C), and a spinel-type M_3O_4 phase (≥500 °C, M represents Ni,Co,Mn). It was also found that this structural transition is accelerated by an increase in the reaction temperature, except at 600 °C, where the thermal decomposition of the $Li_{1-x}MO_{2-y}$ phase inhibited the formation of the M_3O_4 phase. Weight changes of the samples suggested that the chlorination of the transition metals begins at 500 °C and that its rate increases with an increase in the reaction temperature. It was revealed by a composition analysis that an increase in the reaction temperature (except at 600 °C) and longer times result in a higher Li removal ratio. A temperature of 550 °C was proposed as the optimum temperature for the chlorination of NCM in consideration of the findings from this work.

Keywords: Cathode Material, Li-ion Battery, Chlorination, X-ray Diffraction, Recycle

INTRODUCTION

Global efforts are being made to reduce greenhouse gas emissions, with the transportation sector at the forefront of this effort with the help of technological innovation. The proportion of electric vehicles (EVs) among newly registered cars increased by 41% in 2020 [1]. Instead of traditional combustion engines powered by fossil fuels, EVs employ electric motors powered by lithium-ion batteries (LIBs). Due to the increasing demand for LIBs, the production capacity of LIBs is rapidly increasing around the world. However, this movement will eventually face the new issue of waste in the form of used LIBs, as their lifespan is estimated to be 8-10 years in EV applications. Accordingly, a management plan for used LIBs should be established before they cause environmental and social problems. First, used LIBs should be gathered and stored in a specialized location where the toxic chemicals contained in them can be safely managed. In addition, it is worth paying attention to used LIBs in terms of economy, because they are good resources of valuable metals, such as Li, Co, Ni, and Mn, which are used in cathode electrodes.

Various techniques have been developed to recycle used LIBs, including pyrometallurgical, hydrometallurgical, and direct recycling techniques [2-5]. In the pyrometallurgical technique, cathode materials go through a high-temperature process in the range of 1,000-1,500 °C under an oxidizing atmosphere. An alloy ingot of transition metals is achieved via this technique, while other metals such as Li are separated as slag. This technique is commercially available at present, though the high temperature operation and the need for subsequent processes for conversion of the alloy ingot to a form appropriate for re-synthesis are major drawbacks. Acid solutions are generally employed in the hydrometallurgical technique in order to dissolve cathode materials. Techniques such as pH control and the addition of a precipitation reagent are used to recover each constituent metal selectively from the acid solution. This process benefits from the relatively low operation temperature (<95 °C) and the fact that it is widely applied commercially. However, the production of secondary waste, the necessity of an acid solution, and the need for subsequent purification of the recovered metals remain as the key issues to be addressed. The direct recycling technique is focused on the compensation of Li loss which occurs during the use of LIBs. Li can be incorporated into used cathode materials by heating them with a Li source such as LiOH [6,7]. Though this technique is very simple, its applicability to various cathode materials on a large scale needs verification to assess its commercial viability.

Recently, a new technique of chlorination was introduced for the recycling of $Li(Ni_{1/3}Co_{1/3}Mn_{1/3})O_2$ (NCM) [8]. In the chlorination technique, NCM reacts with Cl_2 to convert Li selectively to water-soluble LiCl, while the transition metals remain in their oxide forms. The transition-metal oxides are readily separable by water washing and filtering steps. In the course of chlorination, transition metals partially react with Cl_2 to produce their corresponding chlorides,

†To whom correspondence should be addressed.
E-mail: minku@kaeri.re.kr

which can then be recovered in the subsequent Na_2CO_3 precipitation process. A high transition-metal recovery ratio of 94.9% was achieved through the chlorination technique. It was also reported that NCM can be re-synthesized using the recovered transition metals, demonstrating a capacity of 105 mAh/g. The chlorination technique begins with the chlorination of a cathode material, with this step having a decisive effect on the overall process efficiency. However, the chlorination behavior of NCM has yet to be reported. In this work, the effects of the reaction temperature and time on the chlorination of NCM are investigated.

EXPERIMENTAL

Chlorination experiments were conducted using a quartz tube reactor with a diameter of 40 mm. The reactor was equipped with an electrical furnace in the middle to control the reaction temperature. In the inlet part of the reactor, two mass flow controllers (MFCs) were connected to control the flow rates of Ar (Model 3660, Kofloc Co., Ltd., Japan) and Cl_2 (Model 5400, Kofloc Co., Ltd., Japan) independently. The outlet of the reactor was connected to a dry scrubber which was designed to remove Cl_2 from the exhaust gas stream. After the weighing of 2.00 g of NCM (Ni : Co : Mn= 1 : 1 : 1) purchased from MSE Supplies (USA), it was loaded into an alumina boat. The boat was positioned in the middle of the quartz reactor and the inlet gas flow was then set to 200 mL/min Ar. This condition was maintained for at least 2 h to remove residual air inside the reactor. The electrical furnace began to heat the reactor at a ramping rate of 10 °C/min to the target temperature under an Ar flow. Chlorination was started by changing the Ar and Cl_2 flow rates to 180 and 20 mL/min, respectively. The reaction condition was maintained for the target reaction time and the flow rate of Cl_2 was set to zero. The reactor was then cooled to room temperature. The chlorination experiments were conducted at temperatures of 400, 500, 550, and 600 °C for 1, 2, 4, and 8 h at each temperature. Table 1 presents a list of the samples prepared in this work. The numbers in the sample names indicate the reaction temperature and time: NCM-500-4 represents an NCM sample reacted at 500 °C for 4 h under a 180 mL/min Ar+20 mL/min Cl_2 flow. After chlorination, the samples were immersed in deionized water for at least 15 h and then filtered and dried at 120 °C for 2 h in an oven.

A crystal structural analysis was conducted using X-ray diffraction (XRD, Bruker D2 Phaser) patterns. Inductively coupled plasma-atomic emission spectrometer (ICP-AES, Thermo Scientific iCAP 7400 Duo) and ICP-optical emission spectrometer (ICP-OES, Perkin Elmer, OPTIMA7300DV) were employed to measure the concentrations of transition metals and Li in the samples, respectively.

RESULTS AND DISCUSSION

NCM has a hexagonal crystal structure composed of -Li-O-(Ni,Co,Mn)-O-Li-O-(Ni,Co,Mn)-O- layers stacked along the *c*-axis [9]. The XRD patterns of the NCM-400-1, -2, -4, and -8 specimens are shown in Fig. 1(a) along with the XRD pattern of pristine NCM. Noticeable changes were observed in the H-(006) and H-(108) peaks, which were readily identified in the pristine NCM but not in the NCM specimens regardless of the reaction time. Here, H-(006) represents the (006) peak in the hexagonal structure. The H-(003) peak was subject to a closer look, as shown in Fig. 1(b), to examine changes in the crystal structure. Two peaks were identified in the figure at the 2θ positions of 18.8 (Phase I) and 19.0° (Phase II). The peak position of Phase I was identical to the position of the H-(003) peak in the pristine NCM. An increase in the reaction time resulted in a gradual decrease in the intensity of the Phase I peak, whereas the opposite was observed in the peak of Phase II. These results suggest that the Phase II has a crystal structure similar to that of the pristine NCM with a smaller c parameter and that a structural transition occurs from Phase I to Phase II as the chlorination proceeds. This structural transition was also observed in the H-(104) peak, as shown in Fig. 1(c). A new peak was identified at around 45° (Phase II) and its intensity relative to

Table 1. List of NCM samples prepared in the present study

Sample name	Reaction temperature	Reaction time	Gas flow
NCM-400-1	400 °C	1 h	180 mL/min Ar+20 mL/min Cl_2
NCM-400-2	400 °C	2 h	180 mL/min Ar+20 mL/min Cl_2
NCM-400-4	400 °C	4 h	180 mL/min Ar+20 mL/min Cl_2
NCM-400-8	400 °C	8 h	180 mL/min Ar+20 mL/min Cl_2
NCM-500-1	500 °C	1 h	180 mL/min Ar+20 mL/min Cl_2
NCM-500-2	500 °C	2 h	180 mL/min Ar+20 mL/min Cl_2
NCM-500-4	500 °C	4 h	180 mL/min Ar+20 mL/min Cl_2
NCM-500-8	500 °C	8 h	180 mL/min Ar+20 mL/min Cl_2
NCM-550-1	550 °C	1 h	180 mL/min Ar+20 mL/min Cl_2
NCM-550-2	550 °C	2 h	180 mL/min Ar+20 mL/min Cl_2
NCM-550-4	550 °C	4 h	180 mL/min Ar+20 mL/min Cl_2
NCM-550-8	550 °C	8 h	180 mL/min Ar+20 mL/min Cl_2
NCM-600-1	600 °C	1 h	180 mL/min Ar+20 mL/min Cl_2
NCM-600-2	600 °C	2 h	180 mL/min Ar+20 mL/min Cl_2
NCM-600-4	600 °C	4 h	180 mL/min Ar+20 mL/min Cl_2
NCM-600-8	600 °C	8 h	180 mL/min Ar+20 mL/min Cl_2

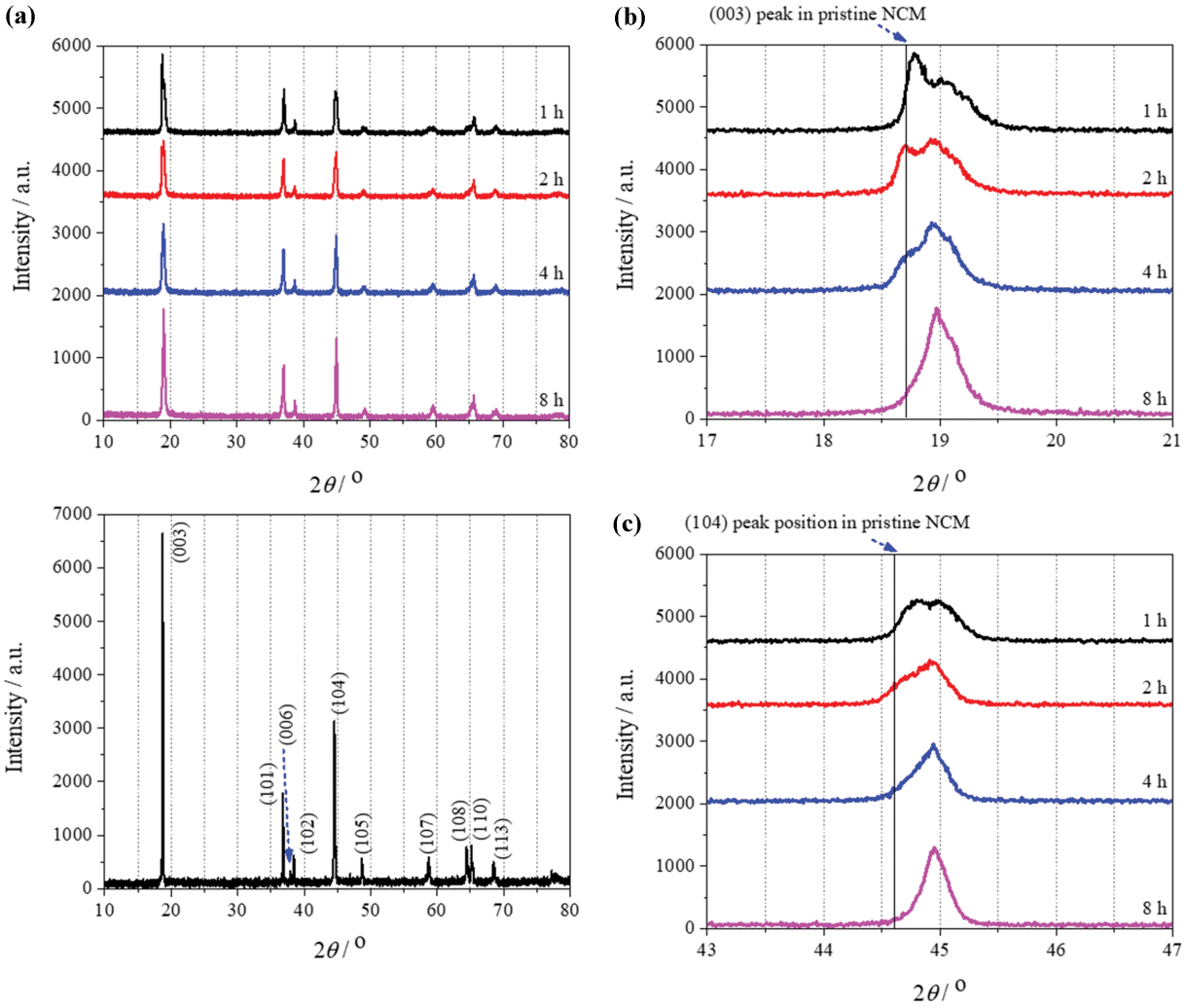

Fig. 1. (a) XRD measurement results of NCM samples reacted at 400 °C for 1, 2, 4, and 8 h under a 180 mL/min Ar+20 mL/min Cl_2 flow. The XRD pattern of pristine NCM is also shown below. Enlarged images of (a) in the 2θ ranges of (b) 17-21° and (c) 43-47°.

the peak on the left (Phase I) increased with an increase in the reaction time. It is important to note that the (104) peak of Phase I was observed at a higher 2θ position than that of the pristine NCM. The lattice parameters of the two phases observed in the NCM-400-1 specimen were calculated using the peak positions. These results are a=2.844 and c=14.17 Å for Phase I and a=2.821 and c=13.99 Å for Phase II. Compared to the values of a=2.863 and c=14.217 Å in the pristine NCM [8], Phase I and II exhibited lattice parameter contraction of around 0.5 and 1.5%, respectively. It was previously reported that the extraction of Li leads to a serial structural transition from a hexagonal phase (H1) to a monoclinic (M), a hexagonal (H2) and a hexagonal (H3) phase [9,10]. During this structural transition, a decrease in the a parameter and an increase in the c/a value was observed. However, the calculated c/a values were 4.98 and 4.96 in Phase I and Phase II, respectively. These values are similar to the value of 4.97 for the pristine NCM, suggesting that the phase transition induced by chlorination does not follow the route identified during the charging-discharging cycles of NCM. The liberation of oxygen atoms during chlorination may account for this difference. Accordingly, the following reaction equations are proposed as a chlorination mechanism of NCM at 400 °C:

$$LiMO_2 + x'/2\ Cl_2(g) \rightarrow Li_{1-x}MO_{2-y'}\ (\text{Phase I}) + x'\ LiCl + y'/2\ O_2(g) \quad (1)$$

$$Li_{1-x}MO_{2-y'} + x''/2\ Cl_2(g) \rightarrow Li_{1-x}MO_{2-y}\ (\text{Phase II}) + x''\ LiCl + y''/2\ O_2(g) \quad (2)$$

where M represents (Ni,Co,Mn), x is (x'+x'') and y is (y'+y'').

When the reaction temperature was increased to 500 °C, the XRD patterns shown in Fig. 2(a) were similar to those observed at 400 °C except that a sign of spinel-type M_3O_4 phase was found at 31.2° in the NCM-500-8 specimen, as denoted by the arrow in the figure. In addition, the highest peak was changed from the H-(003) peak to the peak at 36.7°, which can be assigned to the S-(311) peak from the spinel-oxide phase. These results suggest that the reaction product, the M_3O_4 phase, became the major content in the NCM-500-8 specimen as the chlorination proceeded. Here, it is important to discuss the behavior of the H-(003) peak, as the peak position at 19.0° was kept constant regardless of the reaction time (Fig. 2(b)). This result suggests that Phase II identified at 400 °C is maintained during the M_3O_4 formation. This structural transition was found in the H-(101) peak shown in Fig. 2(c); the peak

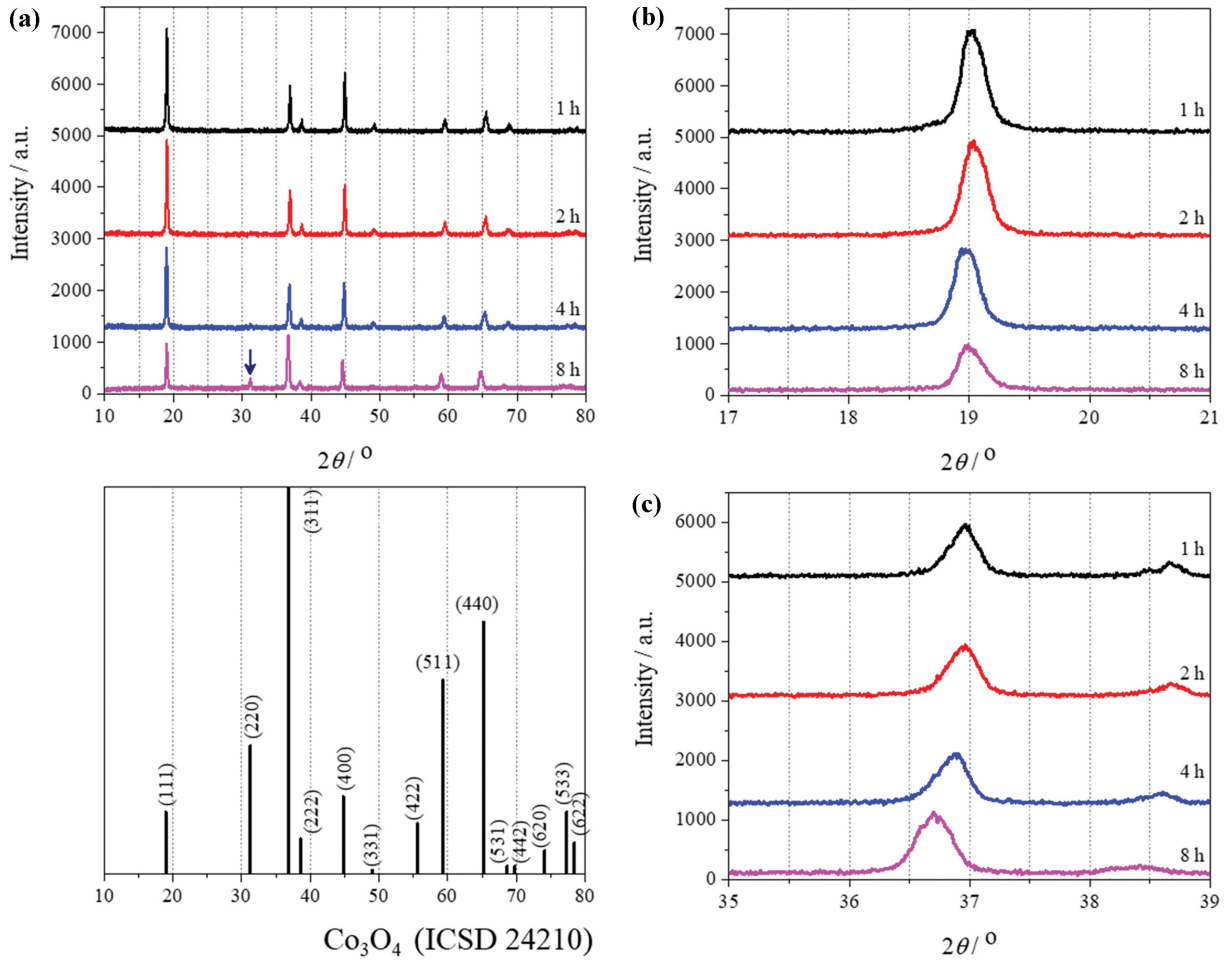

Fig. 2. (a) XRD measurement results of NCM samples reacted at 500 °C for 1, 2, 4, and 8 h under a 180 mL/min Ar+20 mL/min Cl_2 flow. The arrow indicates the (220) peak of the spinel-type M_3O_4 phase. The XRD peak positions of the Co_3O_4 phase (ICSD No. 24210) are also shown below. Enlarged images of (a) in the 2θ ranges of (b) 17-21° and (c) 35-39°.

position was identical at 37.0° in the NCM-500-1 and -2 specimens, which moved to 36.9 and 36.7° in the NCM-500-4 and -8 specimens, respectively. Note that Phase I was not observed after chlorination at 500 °C, indicating that the rate of reaction (2) was profoundly affected by the reaction temperature and was fast at 500 °C. Therefore, the chlorination behavior of NCM at 500 °C can be explained through Eqs. (2) and (3), as shown below.

$$Li_{1-x}MO_{2-y}\ (\text{Phase II}) + (1-x)/2\ Cl_2(g) \rightarrow 1/3\ M_3O_4 + (1-x)\ LiCl + (1/3-y/2)\ O_2(g) \quad (3)$$

To quantify the formation of the M_3O_4 phase, the peak intensity ratio ($I_{(101)}/I_{(003)}$) was derived using the intensity values of the H-(101) and H-(003) peaks. At this point, it should be noted that the H-(101) peak shares the peak position with the S-(311) peak. An $I_{(101)}/I_{(003)}$ ratio of 0.26 was observed in the pristine NCM, which increased to 0.43, 0.46, 0.53 and 1.2 in NCM-500-1, -2, -4, and -8, respectively. The higher $I_{(101)}/I_{(003)}$ ratios in the NCM-500-1 and -2 specimens compared to that of the pristine NCM indicate the formation of the Li-deficient $Li_{1-x}MO_{2-y}$ phase (Phase II). The sudden increase in the $I_{(101)}/I_{(003)}$ ratio observed in NCM-500-8 is in good agreement with the abovementioned findings.

The M_3O_4 phase could be identified even after 1 h of chlorination at 550 °C, as shown in Fig. 3(a). With an increase in the reaction time, a decrease in the intensity of the H-(003) peak was observed, whereas the intensity of the S-(311) peak increased due to the structural transition from the hexagonal $Li_{1-x}MO_{2-y}$ phase to the M_3O_4 phase. This phase transition is also shown in Fig. 3(b), where the H-(101) peak down-shifted to represent the S-(311) peak. In addition, the position of the H-(003) peak moved slightly from 18.9° in the NCM-550-1 specimen to 18.7, 18.7, and 18.6° in the NCM-550-2, -4, and -8 specimens, respectively, as shown in Fig. 3(c). It is important to recall that this peak was observed at 19.0° after chlorination at 500 °C regardless of the reaction time. This result indicates that the identity of this peak was changed from the H-(003) peak of the hexagonal phase to the S-(111) peak of the M_3O_4 phase. The $I_{(101)}/I_{(003)}$ ratios confirmed that proportion of the M_3O_4 phase increased with an increase in the reaction time, resulting in values of 0.71 to 1.5, 1.9, and 2.7 in the NCM-500-1, -2, -4, and -8 samples, respectively. These results show that the reaction mechanism proposed above is applicable at 550 °C and that the reaction rate increases with an increase in the reaction temperature.

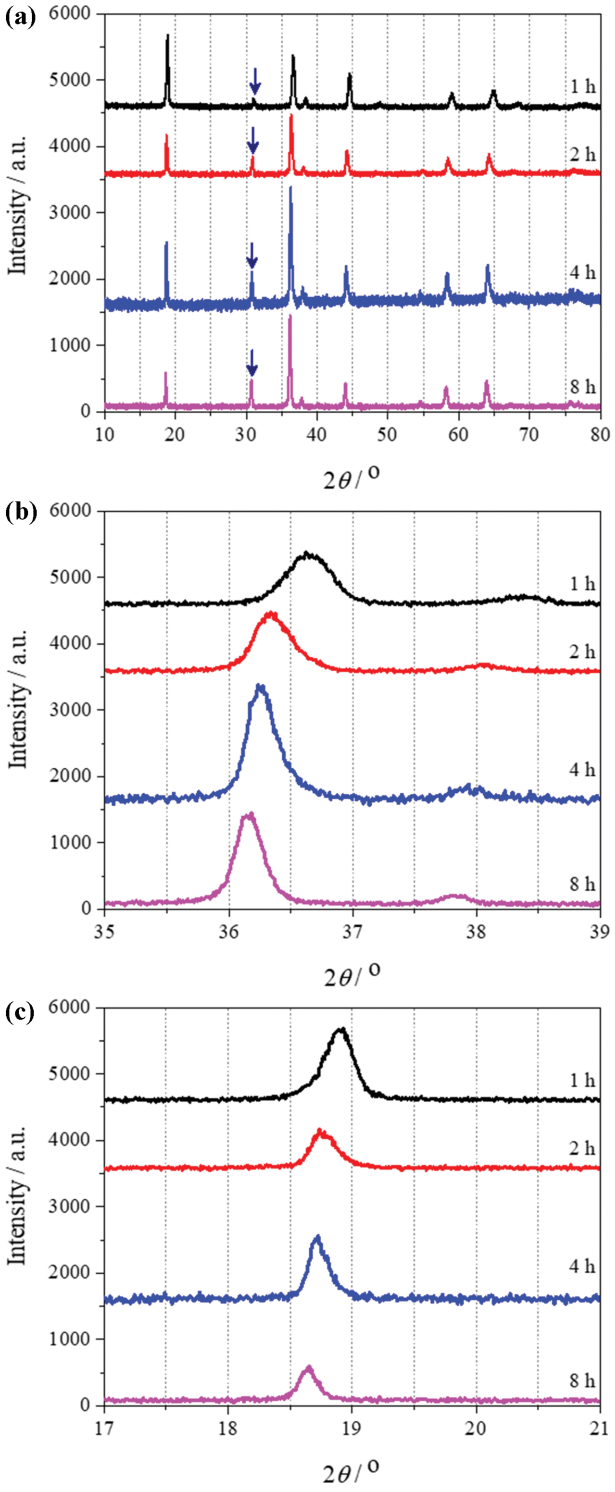

Fig. 3. (a) XRD measurement results of NCM samples reacted at 550 °C for 1, 2, 4, and 8 h under a 180 mL/min Ar+20 mL/min Cl_2 flow. Arrows indicate the (311) peak of the M_3O_4 phase. Enlarged images of (a) in the 2θ ranges of (b) 35-39° and (c) 17-21°.

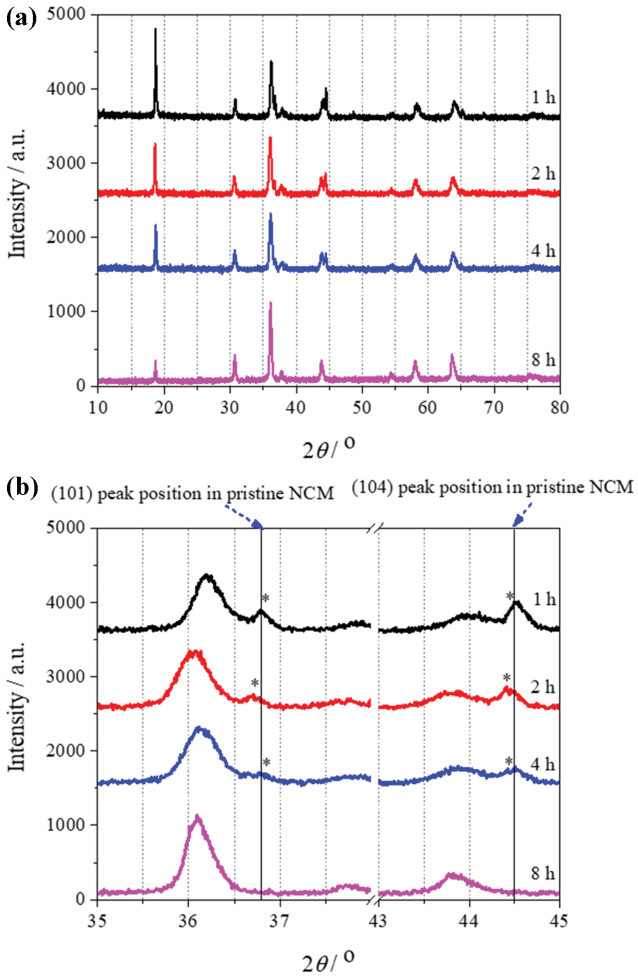

Fig. 4. (a) XRD measurement results of NCM samples reacted at 600 °C for 1, 2, 4, and 8 h under a 180 mL/min Ar+20 mL/min Cl_2 flow. (b) Enlarged image of (a) in the 2θ range of 35-45°.

The formation of the M_3O_4 phase was also observed after chlorination at 600 °C, as shown in Fig. 4(a). An increase in the reaction time resulted in an increase of the $I_{(101)}/I_{(003)}$ ratio from 0.64 in the NCM-600-1 specimen to 1.1, 1.3, and 3.8 in the NCM-600-2, -4, and -8 specimens, respectively. In the reaction time range of 1-4 h, the $I_{(101)}/I_{(003)}$ ratios observed at 600 °C were lower than those at 550 °C; these were 0.71, 1.5, and 1.9 in NCM-550-1, -2, and -4, respectively. However, the result was opposite after 8 h of chlorination, as the ratio was 2.7 in NCM-550-8. In addition to these findings, new peaks were identified at around 36.8 and 44.5°. These peaks are denoted by asterisks in Fig. 4(b). It is interesting that these two peaks can be matched to the H-(101) and H-(104) peaks in the pristine NCM, as shown in the figure. Here, the peak at around 36°, which represents both the H-(101) and S-(311) peaks, behaved similarly to the case at 550 °C. This result means that the chlorination of the $Li_{1-x}MO_{2-y}$ phase to produce the M_3O_4 phase (Eq. (3)) is the dominant reaction. Previously, thermal decomposition of Li-deficient $Li_{0.81}CoO_2$ and $Li_{0.65}CoO_2$ phases was reported to occur at above 250 °C through the following reaction [11]:

$$Li_xCoO_2 \rightarrow x\,LiCoO_2 + (1-x)/3\,Co_3O_4 + (1-x)/3\,O_2(g) \quad (4)$$

Therefore, it is theorized that the following reaction occurred during the chlorination of NCM at 600 °C:

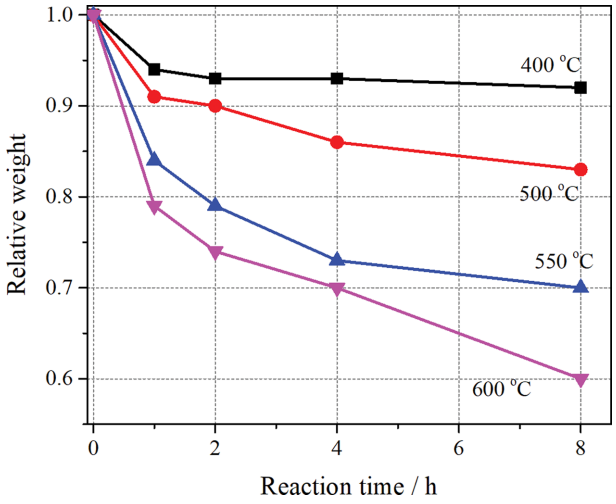

Fig. 5. Effects of the chlorination reaction temperature and time on weight changes in the NCM samples after reaction, water washing, and drying.

$$Li_{1-x}MO_{2-y} \rightarrow (1-x)\ LiMO_2 + x/3\ M_3O_4 + (x/3-y/2)\ O_2(g) \quad (5)$$

This equation suggests that the two reaction mechanisms, chlorination (Eq. (3)) and thermal decomposition (Eq. (5)), compete at 600 °C. The gradual decrease in the peak intensity of the pristine NCM and its relatively low intensity compared to that of the M_3O_4 phase, as observed in Fig. 4(b), indicate that the rate of the thermal decomposition is slower than that of the chlorination process and is decelerated by the continuous consumption of $Li_{1-x}MO_{2-y}$ via chlorination.

The changes in the weight of the NCM samples after chlorination, water washing, filtering, and drying are shown in Fig. 5. As expected from the XRD measurement results, only slight changes were found after chlorination at 400 °C, and the relative weight was 0.92 in NCM-400-8, significantly higher than 0.82, an ideal value based on the complete conversion of NCM into M_3O_4. At 500 °C, the relative weight value gradually decreased with an increase in the reaction time, reaching 0.83 in NCM-500-8. Although this value is close to the ideal value, the presence of the $Li_{1-x}MO_{2-y}$ phase was clearly identified in the XRD measurement results (Fig. 2). Therefore, it is reasonable to assume that the chlorination of the transition metals occurred at 500 °C. It was documented in earlier works that the chlorination of NiO begins at 350 °C and that sublimation of the reaction product, $NiCl_2$, occurs at a temperature exceeding 750 °C [12,13]. For Co, the chlorination of Co_3O_4 was observed at a temperature higher than 300 °C and sublimation of $CoCl_2$ began at 600 °C [14]. An earlier investigation of the chlorination of the Mn oxides of MnO, Mn_3O_4, and Mn_2O_3 found that the reaction began at 270, 380, and 520 °C, respectively [15]. Evaporation of $MnCl_2$, which has a melting point of 650 °C, was observed above 730 °C. According to the literature [12-15], it can be concluded the weight reduction at 500 °C originated from the chlorination of both Li and the transition metals. A significantly faster decrease in the relative weight value was observed when the reaction temperature was increased from 500 to 550 °C. This finding is in line with the XRD measurement results where the formation of the M_3O_4 phase was accelerated at 550 °C. The relative weight value reached 0.70 in NCM-550-8, a value significantly lower than the ideal value, meaning that substantial chlorination of the transition metals occurred. A gradual decrease in the relative weight value was observed in the entire reaction time range at 600 °C. Note that the relative weight values observed at 600 °C were smaller than those of the specimens reacted for identical reaction times at 550 °C. Recalling that the formation of the M_3O_4 phase was decelerated at 600 °C in the reaction time range of 1-4 h due to thermal decomposition, it is suggested that the chlorination of the transition metals was substantially promoted due to the increase in the reaction temperature from 550 to 600 °C.

Here, it is important to discuss the optimum reaction temperature for the chlorination of NCM. According to the XRD measurement results, high proportions of the M_3O_4 phase were achieved at 550 and 600 °C within 8 h of the reaction. However, it was also found that the chlorination of the transition metals occurs at these temperatures. As noted in the Introduction, transition-metal chlorides which dissolve along with LiCl during the water washing process can be recovered via the subsequent steps of the chlorination process [8]. Therefore, the formation of transition-metal chlorides does not harm the overall recovery ratio of the transition metals, whereas a loss by the sublimation or evaporation of the chlorides may require an additional recovery system. The chlorination of the transition metals proceeds faster at 600 °C than at 550 °C according to the relative weight values, with the sublimation of $CoCl_2$ was reportedly beginning at 600 °C [14]. Therefore, it is proposed that the optimum temperature for the chlorination of NCM is 550 °C in order to complete the chlorination within a reasonable reaction time with a high transition-metal recovery ratio.

The effect of chlorination on ratio of transition metals should be discussed here, because each transition metal may react with Cl_2 differently to affect the electrochemical performance of re-synthesized NCM. The ICP-AES result revealed a transition metal ratio of (Ni : Co : Mn)=(0.32 : 0.34 : 0.34) in NCM-550-4, which is similar to that of (0.33 : 0.33 : 0.34) in the pristine NCM [8]. Therefore, it is reasonable to assume that the transition metal ratio was not changed by chlorination under a condition of 550 °C and 4 h. However, it is probable that chlorination under a more severe condition leads to a change in the transition metal ratio.

The amount of Li removed by the chlorination was calculated using the ICP-OES results, as shown in Fig. 6. The Li removal ratio was calculated using the following equation:

$$\text{Li removal ratio} = \text{Removed amount of Li} / \text{Initial amount of Li} \quad (6)$$

It is clear in Fig. 6(a) that an increase in the reaction temperature leads to a higher Li removal ratio in the temperature range of 400-550 °C. However, a further increase in the reaction temperature to 600 °C did not cause noticeable changes, as expected from the XRD measurement results. This result supports the theory that thermal decomposition at 600 °C decelerated the formation of the M_3O_4 phase. The effects of reaction time on the Li removal ratio at 550 °C were also investigated, as shown in Fig. 6(b). Interestingly, it was found that 73% of Li was removed after 1 h of chlorination. The Li removal ratio increased gradually with an increase in the reaction time, reaching 0.96 in NCM-550-8. These results match the find-

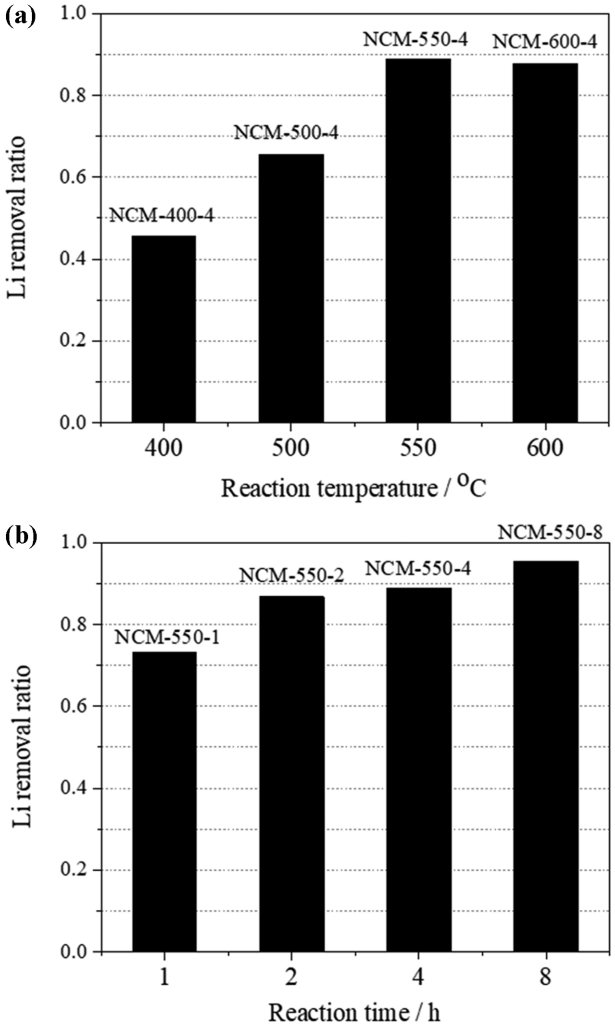

Fig. 6. Effects of the chlorination (a) temperature and (b) time on the Li removal ratio under a 180 mL/min Ar+20 mL/min Cl_2 flow: (a) chlorination conducted for 4 h at each reaction temperature, and (b) chlorination conducted at 550 °C for each reaction time.

ings from the XRD patterns, where the phase transition from the $Li_{1-x}MO_{2-y}$ phase to the M_3O_4 phase proceeded with an increase in the reaction time. Though prolonged chlorination leads to a higher Li removal ratio, the effect of the reaction time weakens as chlorination proceeds. Therefore, from an economical point of view, an optimum condition between the reaction time, i.e., the Li removal ratio, and the electrochemical performance may exist, though this requires further investigation in the near future. In addition, it should be considered that it is difficult to remove Li from NCM completely, and it could be one of the reasons which resulted in a low specific capacity of 105 mAh/g in earlier work [8]. Though chlorination at a more severe condition such as a higher temperature than 600 °C may achieve complete removal of Li, it will lead to loss of transition metals via chlorination and subsequent sublimation/evaporation of their chlorides, as discussed above. Accordingly, it may be reasonable to find an optimum re-synthesis condition to utilize the chlorinated NCM which contains unremoved Li, while keeping the chlorination temperature at 550 °C.

It may be interesting to compare the chlorination behavior of NCM to that of LCO [16]. It was reported that LCO undergoes a structural transition of $LiCoO_2 \rightarrow Li_{1-x}CoO_{2-y} \rightarrow Co_3O_4$ as chlorination proceeds, which is similar to that of NCM except for the absence of the $Li_{1-x}MO_{2-y}$ phase observed at 400 °C. The thermal decomposition of $Li_{1-x}CoO_{2-y}$ was observed at 550 and 600 °C. The effect of thermal decomposition was decisive at 550 °C; the formation of Co_3O_4 was substantially inhibited, resulting in a sudden decrease in the Li removal ratio. Accordingly, the optimum temperature suggested for the chlorination of LCO was 500 °C. These results mean that the chlorination behavior varies significantly depending on the type of cathode material.

CONCLUSION

The chlorination behavior of NCM was investigated at the reaction temperatures of 400, 500, 550, and 600 °C. The step-wise formation of a Li-deficient $Li_{1-x}MO_{2-y}$ phase was observed at 400 °C. The chlorination product changed from the $Li_{1-x}MO_{2-y}$ phase to the spinel-type M_3O_4 phase as the reaction proceeded at 500 °C, and this behavior was accelerated at 550 °C. A further increase in the reaction temperature to 600 °C decelerated the formation of the M_3O_4 phase due to the thermal decomposition of the $Li_{1-x}MO_{2-y}$ phase in the reaction time range of 1-4 h. The optimum temperature for the chlorination of NCM was proposed to be 550 °C in consideration of the fast reaction rate at this temperature and the potential loss of transition metals by sublimation/evaporation at 600 °C.

ACKNOWLEDGEMENTS

This work was sponsored by the "Development of new process for recycling of NCM lithium-ion battery cathode material" project awarded through the KAERI Innovation Challenge program.

REFERENCES

1. International Energy Agency, Global EV Outlook 2021 (2021).
2. T. Or, S. W. D. Gourley, K. Kaliyappan, A. Yu and Z. Chen, *Carbon Energy*, **2**, 6 (2020).
3. G. Harper, R. Sommerville, E. Kendrick, L. Driscoll, P. Slater, R. Stolkin, A. Walton, P. Christensen, O. Heidrich, S. Lambert, A. Abbott, K. Ryder, L. Gaines and P. Anderson, *Nature*, **575**, 75 (2019).
4. H. Bae and Y. Kim, *Mater. Adv.*, **2**, 3234 (2021).
5. S. Refly, O. Floweri, T. R. Mayangsari, A. Sumboja, S. P. Santosa, T. Ogi and F. Iskandar, *ACS Sustainable Chem. Eng.*, **8**, 16104 (2020).
6. P. Xu, Q. Dai, H. Gao, H. Liu, M. Zhang, M. Li, Y. Chen, K. An, Y. S. Meng, P. Liu, Y. Li, J. S. Spangenberger, L. Gains, J. Lu and Z. Chen, *Joule*, **4**, 1 (2020).
7. H. Yang, B. Deng, X. Jing, W. Li and D. Wang, *Waste Manage.*, **129**, 85 (2021).
8. M. K. Jeon, S.-W. Kim, H.-C. Eun, K.-Y. Lee, H. Kim and M. Oh, *Korean J. Chem. Eng.*, **39**, 1472 (2022).
9. L. de Biasi, A. O. Kondrakov, H. Geßwein, T. Brezesinski, P. Hart-

mann and J. Janek, *J. Phys. Chem. C*, **121**, 26163 (2017).
10. Y. Mo, L. Guo, B. Cao, Y. Wang, L. Zhang, X. Jia and Y. Chen, *Energy Storage Mater.*, **18**, 260 (2019).
11. Y. Furushima, C. Yanagisawa, T. Nakagawa, Y. Aoki and N. Muraki, *J. Power Sources*, **196**, 2260 (2011).
12. T. A. Anufrieva, L. E. Derlyukova and M. V. Vinokurova, *Russ. J. Inorg. Chem.*, **46**, 16 (2001).
13. I. Ilić, B. Krstev, K. Cerović and S. Stopić, *Scand. J. Metall.*, **26**, 14 (1997).
14. T. A. Anufrieva and L. E. Derlyukova, *Russ. J. Inorg. Chem.*, **52**, 1840 (2007).
15. G. G. Fouga, G. de Micco and A. E. Bohe, *Thermochim. Acta*, **494**, 141 (2009).
16. M. K. Jeon and S.-W. Kim, *Korean J. Chem. Eng.*, In press (2022). (https://doi.org/10.1007/s11814-022-1117-0).